SHORT COMMUNICATION

Integrating porphyrin-based nanoporous organic polymers with electrochemical aptasensors for ultratrace detection of kanamycin

Guanghui Tian[1] · Feng Guo[1] · Chuanbin Fan[1] · Zi-Ao Zong[1] · Junli Wang[1] · Zhuorigebatu Tegudeer[2] · Wen-Yang Gao[2]

Abstract

The synthesis and characterization of two new porphyrin-based porous organic polymers (POPs) via Sonogashira cross-coupling reaction and leverage the two obtained POPs is reported for the fabrication of electrochemical aptasensors to detect kanamycin at an ultratrace level. The resultant electrochemical aptasensor demonstrates a high linear relationship with the logarithmic value of kanamycin concentration in the range 5×10^{-5}–5 µg/L with the limit of detection of 17.6 pg/L or 36.3 fM. During the analysis of real samples from milk and river, a relative standard deviation of less than 4.39%, and good recovery values in the range 97.0–105% were obtained.

Keywords Porous organic polymers · Electrochemical aptasensors · Electrochemical impedance spectroscopy · Ultratrace detection · Kanamycin

Introduction

Strategies to track down environmental pathways of antibiotics are becoming urgently needed, as their residues being found in underground water, river, soils, and agricultural by-products raise alarming concerns to the ecological system and human health [1, 2]. For instance, kanamycin (KANA), one of the commonly used antibiotics to treat severe bacterial infections and tuberculosis, has left its footprint in a variety of environmental domains. Current methods to detect KANA include enzyme-linked immunosorbent assay [3], high-performance liquid chromatography coupled with various detectors [4], photoelectrochemistry [5], and surface-enhanced Raman spectroscopy [6]. However, these analytical approaches suffer from drawbacks of high cost, limited sensitivity, tedious preprocessing, and complicated time-consuming operations. Thus, an effective and efficient detection tool for KANA is still highly desirable.

Meanwhile, electrochemical aptasensors, a type of biosensors, leverage aptamers as recognition elements and monitor changes of certain electrical signal (i.e., current, impedance, and potential) in response to a recognition event [7]. Due to cooperative behaviors of aptamer binding specificity and the sensitivity of low-cost and fast electrochemical techniques [8–13], electrochemical aptasensors are emerging into an alternative yet promising tool to keep track of antibiotics in the environment.

While several types of materials including graphene, metal–organic frameworks, and gold nanoparticles [14–20] have been employed to immobilize aptamers and amplify the electrochemical output signal, the ongoing development of functional porous organic polymers (POPs) [21, 22], composed of exclusively organic components connected via covalent bonds, leads themselves to be a potential family of candidates to host aptamers [23–26] for the trace detection of KANA, given their remarkable chemical stability, high porosity, and precise synthetic tunability. Herein, we report our systemic work on assembling electrochemical aptasensors using porphyrin-based POPs (PPOPs) for monitoring KANA in real samples at the ultra-trace level. The rationale to exploit the porphyrin as the strut unit is to facilitate the

✉ Feng Guo
guofeng1510@yeah.net

✉ Wen-Yang Gao
gaow@ohio.edu

1   School of Laboratory Medicine, Youjiang Medical University for Nationalities, Baise 533000, Guangxi, China

2   Department of Chemistry and Biochemistry, Ohio University, Athens, OH 45701, USA

formation of rigid and significant pore space and the immobilization of aptamers via intermolecular π–π stacking.

Experimental

We started the assembly of electrochemical aptasensors by synthesizing two porphyrin-based POPs via Sonogashira cross-coupling chemistry between the porphyrin-containing polyalkyne and aryl iodides (Fig. 1a). In particular, the coupling reaction was carried out using a mixture of 5,10,15,20-tetrakis(4-ethynylphenyl)-21H,23H-porphine (TEPP, 0.75 equiv) with 1,3,5-triiodobenzene (TIB, 1.0 equiv) or 2,4,6-triiodophloroglucinol (TIP, 1.0 equiv) in 1:1 (v/v) N,N-dimethylformamide (DMF) and triethylamine, which was heated at 105 °C for 48 h under a N_2 atmosphere (see details in Supplementary Information, SI). The harvested purple powder solids (Figure S1), PPOP-H from the monomer of TIB and PPOP-OH from TIP, did not dissolve in any common solvents, such as DMF, tetrahydrofuran, methanol, or H_2O. Extensive washing procedures were applied to the obtained solids using the above solvents, as well as 0.1 M aqueous HCl solution, to remove potential residues. The obtained PPOPs serve as potential candidates to immobilize aptamers and thus lead to electrochemical aptasensors for sensing KANA (Fig. 1b).

Results and discussion

The successful high-degree polymerization reactions were monitored by both solid-state ^{13}C cross-polarization magic angle spinning (CP MAC) nuclear magnetic resonance (NMR) and infrared (IR) spectroscopy. As shown in Figure S2, both PPOP-H and PPOP-OH display signals between 110 and 154 ppm corresponding to aromatic carbons from porphyrin and phenyl motifs. The relatively broad peak around 76 ppm is ascribed to –C≡C– fragment in the skeleton. IR spectra (Fig. 2a) indicate disappearances of terminal alkyne C–H vibration around 3270 cm^{-1} from TEPP and C–I stretch around 600 cm^{-1} from TIB and TIP in the obtained polymers. On the basis of power X-ray diffraction analysis (Figures S3 and S4), PPOP-OH and PPOP-H are amorphous materials in the absence of any diffraction peaks, which is consistent with previous reports that Sonogashira cross-coupling reactions provide access to amorphous POPs due to the irreversibility nature of their reactions [27, 28]. Thermogravimetric analysis (TGA, Figures S5 and S6) reveals that both POPs are thermally stable to above 320 °C after which continuous weight loss is observed.

To investigate their porosity, N_2 adsorption isotherms at 77 K (Fig. 2b) were collected on samples of PPOP-H
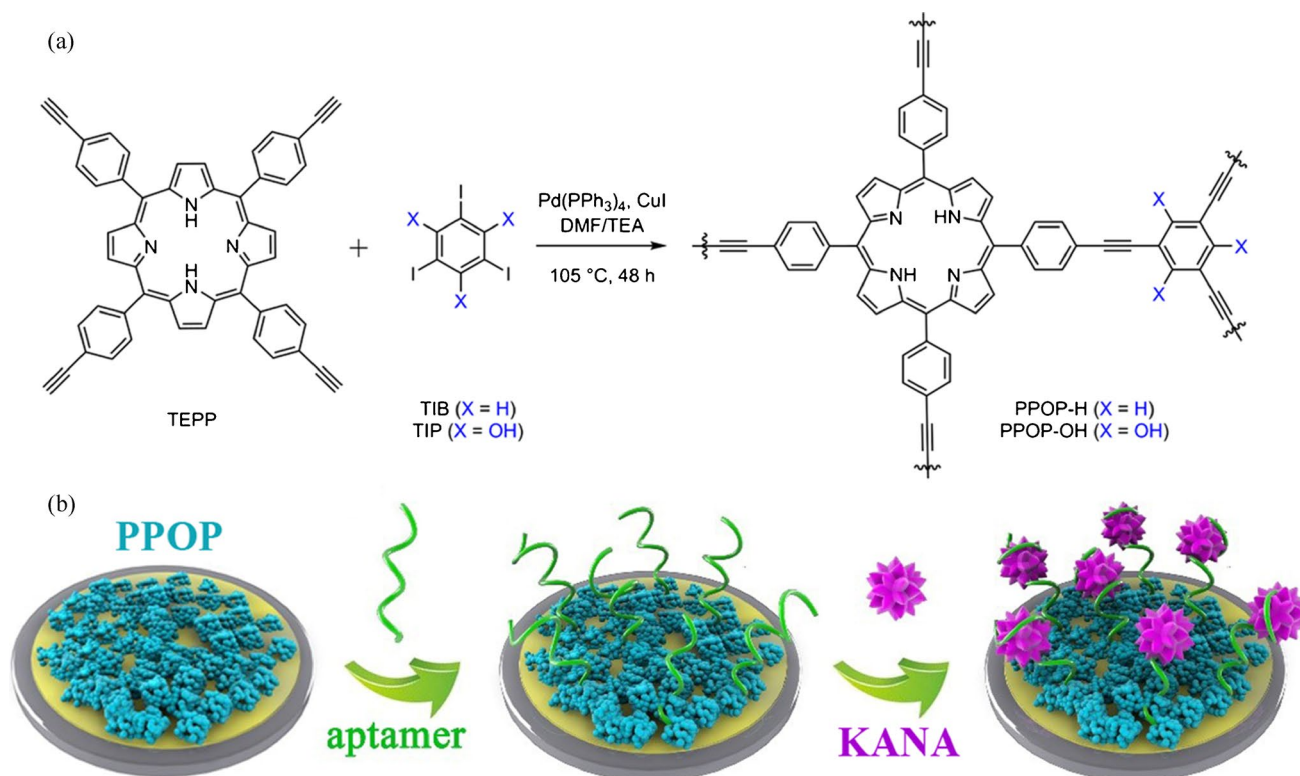

Fig. 1 **a** Two porphyrin-based porous organic polymers were prepared by Sonogashira cross-coupling chemistry. **b** An illustration of fabricating PPOP-based electrochemical aptasensors for detecting KANA
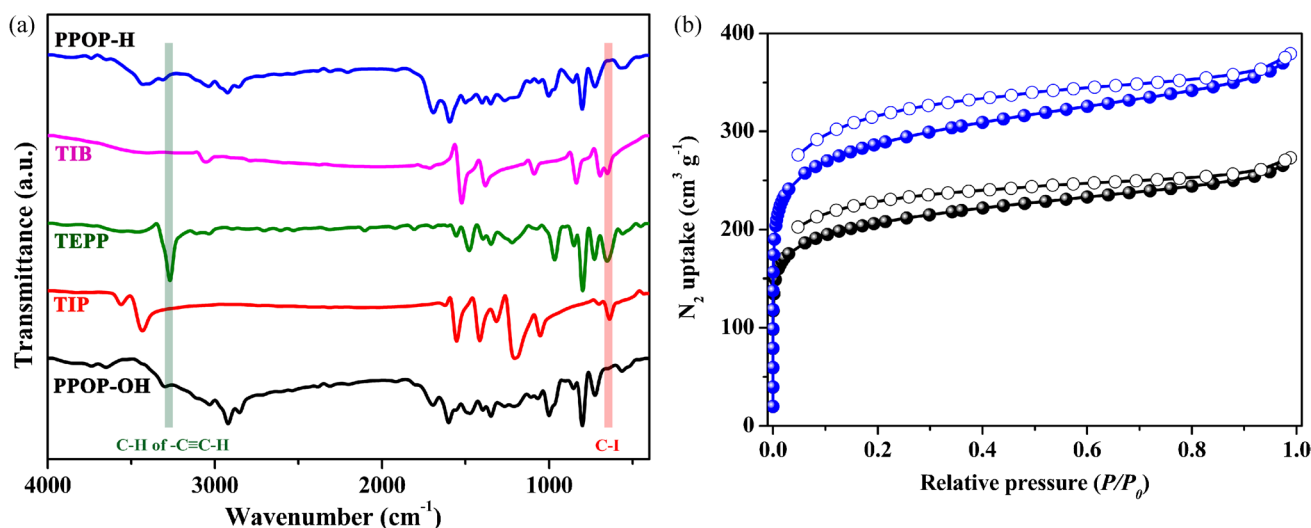
Fig. 2 **a** IR spectra indicate disappearances of terminal alkyne C–H vibration around 3270 cm^{-1} from TEPP and C–I stretch around 600 cm^{-1}. from TIB and TIP in the obtained polymers. **b** N$_2$ adsorption isotherms at 77 K were collected on samples of PPOP-H (blue line) and PPOP-OH (black line)

and PPOP-OH, which were pre-exchanged by dichloromethane and further activated under vacuum at 120 °C for 10 h. Brunauer–Emmet–Teller (BET) surface areas are calculated as 701 m^2/g and 976 m^2/g (P/P$_0$ = 0.05–0.25) for PPOP-OH and PPOP-H, respectively. Furthermore, their pore size distributions in Figure S7 derived from N$_2$ adsorption isotherms show both samples feature hierarchical pores. Scanning electron microscopy (SEM) and transmission electron microscopy (TEM) were also employed to observe the morphologies and microstructures, which show that obtained PPOPs are crosslinked amorphous nanoparticles (Figure S8).

Given the features of high stability and hierarchical pores along with extended conjugated motifs, the obtained two PPOPs were readily used to modify the surface of Au electrode (AE) to obtain PPOP@AE, which were then immersed in the aptamer solution to build the titled PPOP-based electrochemical aptasensors (apt@PPOP@AE, see details in SI). Electrochemical impedance spectroscopy (EIS) Nyquist plots were simulated by the Randles equivalent circuit (Figure S9) [29]. The R_{ct} changes ($\Delta R_{ct} = R_{ct,PPOP@AE} - R_{ct,AE}$ and $\Delta R_{ct} = R_{ct,apt@PPOP@AE} - R_{ct,PPOP@AE}$) were calculated from a series of screening experiments to obtain optimal preparation conditions. For instance, in the case of apt@PPOP-OH@AE, different amounts of PPOP-OH were loaded on the surface of AEs. As shown in Figure S10, the ΔR_{ct} value of PPOP-OH@AE increases to 60 Ω after adding 10 μL of PPOP-OH (0.20 mg/mL in methanol), but no significant increase can be found with the further addition of PPOP-OH. Additionally, the ΔR_{ct} value of apt@PPOP-OH@AE (Figure S11) was significantly enhanced by extending its soaking time in the aptamer solution at 10.0 ng/mL for 2 h.

Thus, those results offer the optimal preparation condition to prepare the PPOP-OH-based electrochemical aptasensor.

To better understand the fabricated PPOP-OH-based electrochemical aptasensor, a suite of solid-state characterizations was applied to the composite samples, apt@PPOP-OH or apt@PPOP-OH@AE. High-angle annular dark field-scanning transmission electron microscopy (HAADF-STEM) coupled with energy-dispersive X-ray spectroscopy (EDX) shows that C and N elements are well dispersed on apt@PPOP-OH (Figures S12a–c). Meanwhile, the P element from aptamer is also uniformly dispersed throughout the sample (Figure S12d), which confirms the successful fabrication of apt@PPOP-OH via immersion. X-ray photoelectron spectroscopy (XPS) was employed to probe the carbon electronic states of PPOP-H and apt@PPOP-H. As seen in Figure S12e, the high-resolution C1s XPS spectrum of PPOP-OH can be well deconvoluted into three peaks at 284.4 eV (C–C/C–H), 285.5 eV (C–O), and 287.4 eV (C–N=C). Nevertheless, four separate peaks are found in apt@PPOP-OH, including 284.4 eV (C–C/C–H), 285.5 eV (C–O), 287.3 eV (C–N=C), and 291.1 eV (π–π) (Figure S12f). The additional peak at 291.1 eV indicates that aptamers are immobilized on PPOP-OH via the π–π interaction, which is consistent with the previous report [30].

The obtained electrochemical aptasensor, apt@PPOP-OH@AE, was employed to probe KANA. EIS Nyquist plots were used to monitor the electrochemical signal change during the manufacturing and testing processes. As shown in Figure S13, apt@PPOP-OH@AE displays larger EIS Nyquist plots than PPOP-OH@AE ($\Delta R_{ct} = R_{ct,apt@PPOP-OH@AE} - R_{ct,PPOP-OH@AE} = 58.4$ Ω). Moreover, the KANA (50 pg/L or 0.05 ppt) treated apt@

PPOP-OH@AE sample shows expanded EIS Nyquist plots relative to apt@PPOP-OH@AE itself ($\Delta R_{ct} = R_{ct,KANA@apt@PPOP-OH@AE} - R_{ct,\ apt@PPOP-OH@AE} = 120.2\ \Omega$). These data unambiguously highlight that the PPOP-OH-based electrochemical aptasensor is successfully applied to detect KANA. Furthermore, the interaction with KANA was reflected on the C1s XPS signal of KANA-loaded apt@PPOP-OH (Figure S12g), which is deconvoluted into four peaks of 284.4 eV (C–C/C–H), 285.9 eV (C–O/C–N), 288.1 eV (C–N=C/C=O), and 291.1 eV (π–π). Compared with apt@PPOP-OH, the slight shifts of peaks are probably attributed to the addition of KANA. Based on the same fabrication procedures, we prepared another electrochemical aptasensor using PPOP-H, apt@PPOP-H@AE. EIS Nyquist plots of the PPOP-H-based electrochemical aptasensor (Figure S14) show performances similar to those of the PPOP-OH-based aptasensor. However, the corresponding ΔR_{ct}

values (Fig. 3a) of the PPOP-H-based aptasensor are significantly lower than ones of the PPOP-OH-based aptasensor, which is mainly attributed to the relatively strong interaction between aptamer and the –OH functional group in PPOP-OH. Thus, the following studies were carried out by focusing on apt@PPOP-OH@AE for the detection of KANA.

The electrochemical aptasensor, apt@PPOP-OH@AE, was incubated separately in a series of KANA solutions at different concentrations to evaluate its sensitivity. As seen in Fig. 3b, the EIS Nyquist plots were enhanced appreciably and stepwise upon increasing the KANA concentration, which generated a G-quadruplex complex between KANA and aptamer. The R_{ct} change ($\Delta R_{ct} = R_{ct,KANA@apt@PPOP-OH@AE} - R_{ct,apt@PPOP-OH@AE}$) was used as the responsive signal to detect KANA. This ΔR_{ct} value exhibits a great linear relationship with the logarithmic value of KANA concentration in the range of 5×10^{-5}–5 µg/L
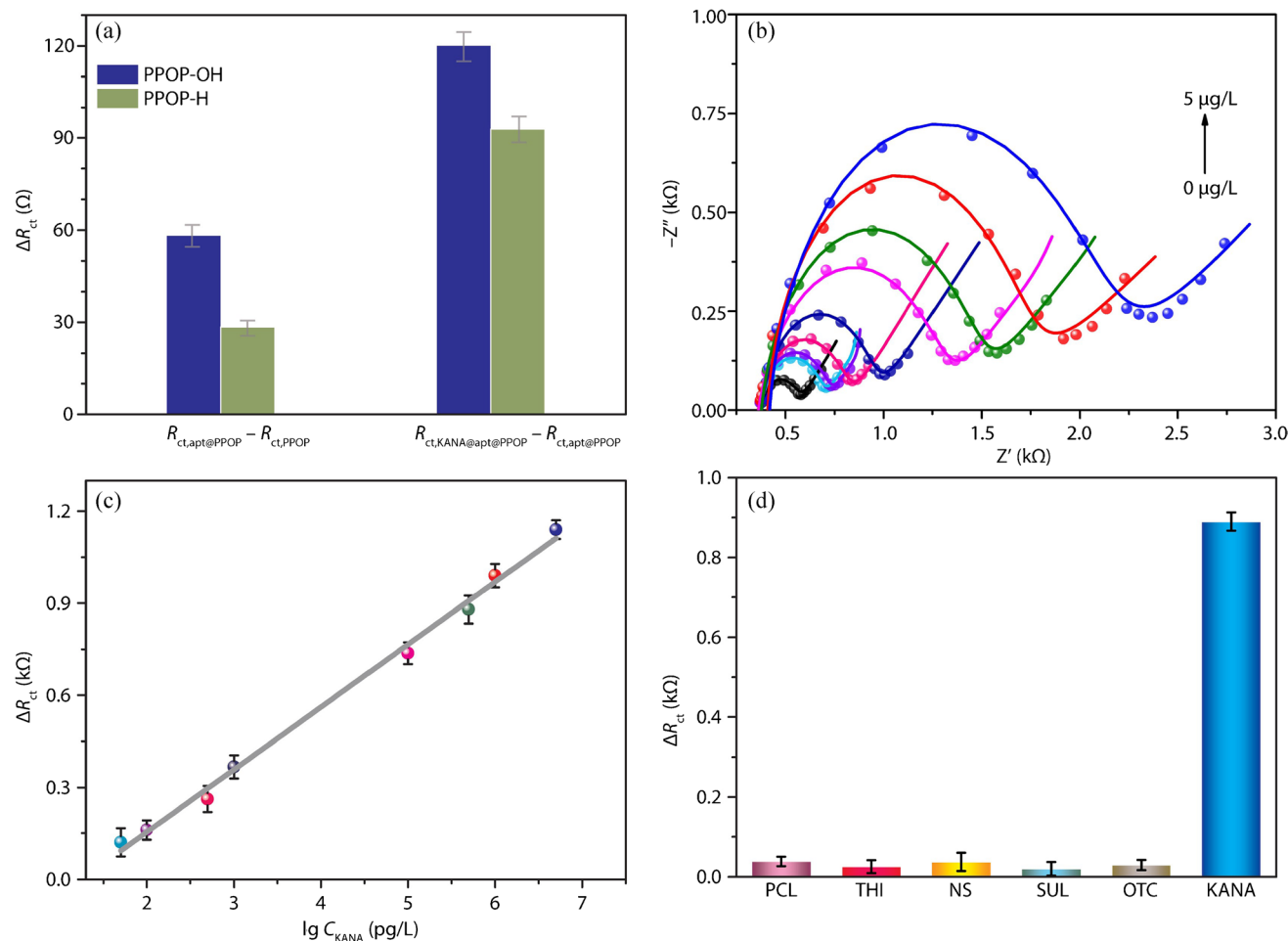

Fig. 3 a Comparison of the ΔR_{ct} values of PPOP-OH and PPOP-H-based aptasensors indicates the relatively high sensitivity using PPOP-OH. **b** EIS Nyquist plots of the PPOP-OH-based electrochemical aptasensor in different KANA concentrations. **c** The linear rela-

tionship between the ΔR_{ct} value and the logarithmic value of KANA concentration. **d** The selectivity of the fabricated PPOP-OH-based electrochemical aptasensor for detecting KANA in the presence of various interferences at 0.5 µg/L

Table 1 The obtained electrochemical aptasensor, apt@PPOP-OH@AE, demonstrates superior sensing performance for KANA than other testing methods

Materials	Test method	Detection range	LOD	Ref
Au/SD-TiO$_2$ NT	Amperometric	0.2–200 nM	0.1 nM	[31]
GO/w-g-C$_3$N$_4$	Photocurrent	1–230 nM	0.2 nM	[32]
Conducting polymer/Au nanocomposite	Linear sweep voltammetry	0.05–9 μM	9.4 nM	[33]
Imprinted boronic acid-functionalized Au NP composite	Surface plasmon resonance	1–1000 pM	1 pM	[34]
GO/Au NP nanocomposite	Surface-enhanced Raman scattering	1–100 nM	0.75 nM	[35]
Molecularly imprinted polymer	Surface plasmon resonance	0.1–10 μM	12 nM	[36]
TiO$_2$-MoS$_2$-Au NP heterostructure	Photoelectrochemical aptasensor	0.2–450 μM	50 pM	[37]
Carbon black-oligolactide composite	Electrochemical impedance spectroscopy	0.7–50 nM	0.3 nM	[38]
PPOP-OH	Electrochemical impedance spectroscopy	1.03×10^{-4}–10.3 nM	36.3 fM	This work

(or ppb). The corresponding linear regression equation is $\Delta R_{ct} = 0.204(\pm 0.006) \times \lg C_{KANA} - 0.25(\pm 0.02)$ with the determination coefficient (R^2) of 0.995 (Fig. 3c). The limit of detection (LOD) is calculated to be 17.6 pg/L or 36.3 fM with a signal-to-noise ratio of 3 through the simulated linear regression equation, which is significantly superior than other reported sensors (see the summary in Table 1) [31–38].

The reproducibility of apt@PPOP-OH@AE was confirmed by four parallel electrodes for impedimetric aptasensing of KANA at 0.5 μg/L, which have similar ΔR_{ct} values with a relative standard deviation (RSD) below 4.7% (Figure S15). Moreover, the selectivity of apt@PPOP-OH@AE was studied by analyzing the ΔR_{ct} values of the apt@PPOP-OH@AE in KANA and various interferences (Fig. 3d), including penicillin (PCL), thiamphenicol (THI), neomycin sulfate (NS), sulfapyridine (SUL), and oxytetracycline (OTC). The electrochemical aptasensor shows the maximum ΔR_{ct} value for detecting KANA (0.5 μg/L), while the negligible variation was found for these interferences at the same concentration (0.5 μg/L), which reveals its excellent selectivity toward KANA. The fabricated aptasensor after monitoring KANA (0.5 μg/L) can be retained well at -20 °C for 10 days to ascertain the acceptable stability, as displayed in Figure S16. Hence, the PPOP-OH-based electrochemical aptasensor has high selectivity, fine reproducibility, and acceptable stability in the detection of KANA.

Detection of KANA in real samples is an important step to assess the practical applicability of sensors. Here we employed samples of milk and river to investigate the detection capability of apt@PPOP-OH@AE. The electrochemical aptasensor was immersed in real samples together with different amounts of KANA to collect EIS Nyquist plots (see details in S1). As summarized in Table S1, the measured number of KANA is consistent well with the actual KANA addition at 0.100, 1.00, and 100 ng/L with a low RSD (<4.39%) and a recovery value in the range of 97.0–105%. Therefore, the PPOP-OH-based electrochemical aptasensor

illustrates its applicability to detect KANA in various real samples. However, the spent electrochemical aptasensor is a little difficult to restore the original sensing ability by immersing in the distilled water, which may be complicated various factors including strong interactions between aptamers and KANA and KANA being trapped in POPs.

Conclusion

In conclusion, we not only reported the synthesis and characterization of two porphyrin-based porous organic polymers, but also employed them to build electrochemical aptasensors to detect KANA. Thanks to the existence of hydroxyl functional groups as well as hierarchical pores and extended conjugated motifs, the PPOP-OH-based electrochemical aptasensor shows remarkable impedimetric sensing for ultratrace KANA even in various real samples. The fabricated aptasensor has ultrahigh sensitivity, outstanding selectivity, available reproducibility, and impressive stability. We expect that this research paves a promising avenue to develop highly sensitive electrochemical aptasensors toward ultratrace analytes.

Data Availability All data generated or analysed during this study are included in this published article and its supplementary information file.

Declarations

References

1. Danner MC, Robertson A, Behrends V, Reiss J (2019) Antibiotic pollution in surface fresh waters: occurrence and effects. Sci Total Environ 664:793–804. https://doi.org/10.1016/j.scitotenv.2019.01.406

2. Ben Y, Fu C, Hu M, Liu L, Wong MH, Zheng C (2019) Human health risk assessment of antibiotic resistance associated with antibiotic residues in the environment: a review. Environ Res 169:483–493. https://doi.org/10.1016/j.envres.2018.11.040

3. Chen Y, Wang Z, Wang Z, Tang S, Zhu Y, Xiao X (2008) Rapid enzyme-linked immunosorbent assay and colloidal gold immunoassay for kanamycin and tobramycin in swine tissues. J Agric Food Chem 56:2944–2952. https://doi.org/10.1021/jf703602b

4. See a broad array of detectors including UV/fluorescence, evaporative light scattering detector/pulsed electrochemical detection, and mass spectrometry coupled with HPLC for kanamycin analysis in the following reference. Zhang X, Wang J, Wu Q, Li L, Wang Y, Yang H (2019) Determination of kanamycin by high performance liquid chromatography. Molecules 24:1902. https://doi.org/10.3390/molecules24101902

5. Huang Z, Li Z, Chen Y, Xu L, Xie Q, Deng H, Chen W, Peng H (2021) Regulating valence states of gold nanocluster as a new strategy for the ultrasensitive electrochemiluminescence detection of kanamycin. Anal Chem 93:4635–4640. https://doi.org/10.1021/acs.analchem.1c00063

6. Liang JF, Peng C, Li P, Ye QX, Wang Y, Yi YT, Yao ZS, Chen GY, Zhang BB, Lin JJ, Luo Q, Chen X (2021) A review of detection of antibiotic residues in food by surface-enhanced Raman spectroscopy. Bioinorg Chem Appl 2021:8180154. https://doi.org/10.1155/2021/8180154

7. Radi AE, Abd-Ellatief MR (2021) Electrochemical aptasensors: current status and future perspectives. Diagnostics 11:104. https://doi.org/10.3390/diagnostics11010104

8. Mu Z, Tian J, Wang J, Zhou J, Bai L (2022) A new electrochemical aptasensor for ultrasensitive detection of endotoxin using Fe-MOF and AgNPs decorated P-N-CNTs as signal enhanced indicator. Appl Surf Sci 573:151601. https://doi.org/10.1016/j.apsusc.2021.151601

9. Wang S, He B, Liang Y, Jin H, Wei M, Ren W, Suo Z, Wang J (2021) Exonuclease III-driven dual-amplified electrochemical aptasensor based on PDDA-Gr/PtPd@Ni-Co hollow nanoboxes for chloramphenicol detection. ACS Appl Mater Interfaces 13:26362–26372. https://doi.org/10.1021/acsami.1c04257

10. Hu J, Wu D, Li T, Cao Y, Wang X, Gan N (2022) Ratiometric electrochemical aptasensor for point-of-care testing Vibrio parahaemolyticus together with antimicrobial peptide-labeled nano metal-organic framework signal tag. Sen Actuators B Chem 352:130987. https://doi.org/10.1016/j.snb.2021.130987

11. Zhang HW, Zhu QQ, Yuan R, He H (2021) Crystal engineering of MOF@COF core-shell composites for ultra-sensitively

12. Wen XH, Zhao XF, Peng BF, Yuan KP, Li XX, Zhu LY, Lu HL (2021) Facile preparation of an electrochemical aptasensor based on Au NPs/graphene sponge for detection of homocysteine. Appl Surf Sci 556:149735. https://doi.org/10.1016/j.apsusc.2021.149735

13. Wadhwa S, John AT, Nagabooshanam S, Mathur A, Narang J (2020) Graphene quantum dot-gold hybrid nanoparticles integrated aptasensor for ultra-sensitive detection of vitamin D3 towards point-of-care application. Appl Surf Sci 521:146427. https://doi.org/10.1016/j.apsusc.2020.146427

14. Chen M, Li H, Su X, Wu R, Feng H, Shi X, Liang J, Chen J, Li G (2021) Label-free electrochemical aptasensor based on reduced graphene oxide–hemin–chitosan nanocomposite for the determination of glypican-3. New J Chem 45:8608–8618. https://doi.org/10.1039/D1NJ00633A

15. Ma D, Liu J, Liu H, Yi J, Xia F, Tian D, Zhou C (2022) Multiplexed electrochemical aptasensor based on mixed valence Ce(III, IV)-MOF for simultaneous determination of malathion and chlorpyrifos. Anal Chim Acta 1230:340364. https://doi.org/10.1016/j.aca.2022.340364

16. Fan L, Zhao G, Shi H, Liu M, Li Z (2013) A highly selective electrochemical impedance spectroscopy-based aptasensor for sensitive detection of acetamiprid. Biosens Bioelectron 43:12–18. https://doi.org/10.1016/j.bios.2012.11.033

17. Wei P, Wang S, Wang W, Niu Z, Rodas-Gonzalez A, Li K, Li L, Yang Q (2022) CoNi bimetallic metal–organic framework and gold nanoparticles-based aptamer electrochemical sensor for enrofloxacin detection. Appl Surf Sci 604:154369. https://doi.org/10.1016/j.apsusc.2022.154369

18. Zhang Y, Liu M, Pan S, Yu L, Zhang S, Liu R (2022) A magnetically induced self-assembled and label-free electrochemical aptasensor based on magnetic Fe_3O_4/Fe_2O_3@Au nanoparticles for $VEGF_{165}$ protein detection. Appl Surf Sci 580:152362. https://doi.org/10.1016/j.apsusc.2021.152362

19. Lu H, Huang Y, Cui H, Li L, Ding Y (2022) A molecularly imprinted electrochemical aptasensor based on zinc oxide and co-deposited gold nanoparticles/reduced graphene oxide composite for detection of amoxicillin. Microchim Acta 189:421. https://doi.org/10.1007/s00604-022-05497-x

20. Zhang HW, Li HK, Han ZY, Yuan R, He H (2022) Incorporating fullerenes in nanoscale metal–organic matrixes: an ultrasensitive platform for impedimetric aptasensing of tobramycin. ACS Appl Mater Interfaces 14:7350–7357. https://doi.org/10.1021/acsami.1c23320

21. Chaoui N, Trunk M, Dawson R, Schmidt J, Thomas A (2017) Trends and challenges for microporous polymers. Chem Soc Rev 46:3302–3321. https://doi.org/10.1039/C7CS00071E

22. Sun Q, Dai Z, Meng X, Xiao FS (2015) Porous polymer catalysts with hierarchical structures. Chem Soc Rev 44:6018–6034. https://doi.org/10.1039/C5CS00198F

23. Han ZY, Li HK, Zhu QQ, Yuan R, He H (2021) An intriguing electrochemical impedance aptasensor based on a porous organic framework supported silver nanoparticles for ultrasensitively detecting theophylline. Chin Chem Lett 32:2865–2868. https://doi.org/10.1016/j.cclet.2021.02.013

24. Dong S, Zhang J, Huang G, Wei W, Huang T (2021) Conducting microporous organic polymer with –OH functional groups: special structure and multi-functional integrated property for organophosphorus biosensor. Chem Eng J 405:126682. https://doi.org/10.1016/j.cej.2020.126682

25. Yuan R, Yan Z, Shaga A, He H (2021) Design and fabrication of an electrochemical sensing platform based on a porous organic polymer for ultrasensitive ampicillin detection. Sen Actuators B Chem 327:128949. https://doi.org/10.1016/j.snb.2020.128949

26. Han ZY, Zhu QQ, Zhang HW, Yuan R, He H (2020) A porous organic framework composite embedded with Au nanoparticles: an ultrasensitive electrochemical aptasensor toward detection of oxytetracycline. J Mater Chem C 8:14075–14082. https://doi.org/10.1039/D0TC03769A

27. Gao WY, Ezazi AA, Wang CH, Moon J, Abney C, Wright J, Powers DC (2019) Metallopolymerization as a strategy to translate ligand-modulated chemoselectivity to porous catalysts. Organometallics 38:3436–3443. https://doi.org/10.1021/acs.organomet.9b00162

28. Jiang JX, Su F, Trewin A, Wood CD, Niu H, Jones JTA, Khimyak YZ, Cooper AI (2008) Synthetic control of the pore dimension and surface area in conjugated microporous polymer and copolymer networks. J Am Chem Soc 130:7710–7720. https://doi.org/10.1021/ja8010176

29. Zhu QQ, Li HK, Sun XL, Han ZY, Sun J, He H (2021) Rational incorporation of covalent organic framework/carbon nanotube (COF/CNT) composites for electrochemical aptasensing of ultratrace atrazine. J Mater Chem C 9:8043–8050. https://doi.org/10.1039/D1TC01506K

30. Han ZY, Zhang H, Li HK, Zhu QQ, He H (2021) Ingenious construction of an electrochemical aptasensor based on a Au@COF/GO-NH$_2$ composite with excellent detection performance. J Mater Chem C 9:4576–4582. https://doi.org/10.1039/D1TC00319D

31. Xin Y, Li Z, Zhang Z (2015) Photoelectrochemical aptasensor for the sensitive and selective detection of kanamycin based on Au nanoparticle functionalized self-doped TiO$_2$ nanotube arrays. Chem Commun 51:15498–15501. https://doi.org/10.1039/C5CC05855D

32. Li R, Liu Y, Cheng L, Yang C, Zhang J (2014) Photoelectrochemical aptasensing of kanamycin using visible light-activated carbon nitride and graphene oxide nanocomposites. Anal Chem 86:9372–9375. https://doi.org/10.1021/ac502616n

33. Zhu Y, Chandra P, Song KM, Ban C, Shim YB (2012) Label-free detection of kanamycin based on the aptamer-functionalized conducting polymer/gold nanocomposite. Biosens Bioelectron 36:29–34. https://doi.org/10.1016/j.bios.2012.03.034

34. Frasconi M, Tel-Vered R, Riskin M, Willner I (2010) Surface plasmon resonance analysis of antibiotics using imprinted boronic acid-functionalized au nanoparticle composites. Anal Chem 82:2512–2519. https://doi.org/10.1021/ac902944k

35. Nguyen AH, Ma X, Park HG, Sim SJ (2019) Low-blinking SERS substrate for switchable detection of kanamycin. Sen Actuators B Chem 282:765–773. https://doi.org/10.1016/j.snb.2018.11.037

36. Zhang L, Zhu C, Chen C, Zhu S, Zhou J, Wang M, Shang P (2018) Determination of kanamycin using a molecularly imprinted SPR sensor. Food Chem 266:170–174. https://doi.org/10.1016/j.foodchem.2018.05.128

37. Liu X, Liu P, Tang Y, Yang L, Li L, Qi Z, Li D, Wong DKY (2018) A photoelectrochemical aptasensor based on a 3D flower-like TiO2-MoS2-gold nanoparticle heterostructure for detection of kanamycin. Biosens Bioelectron 112:193–201. https://doi.org/10.1016/j.bios.2018.04.041

38. Kulikova T, Gorbatchuk V, Stoikov I, Rogov A, Evtugyn G, Hianik T (2020) Impedimetric determination of kanamycin in milk with aptasensor based on carbon black-oligolactide composit. Sensors 20:4738. https://doi.org/10.3390/s20174738